J Mol Model (2013) 19:1237–1250
DOI 10.1007/s00894-012-1664-0

ORIGINAL PAPER

Comparison of the structural characteristics of Cu^{2+}-bound and unbound α-syn12 peptide obtained in simulations using different force fields

Zanxia Cao · Lei Liu · Liling Zhao · Haiyan Li · Jihua Wang

Received: 5 September 2012 / Accepted: 23 October 2012 / Published online: 18 November 2012

Abstract The effects of Cu^{2+} binding and the utilization of different force fields when modeling the structural characteristics of α-syn12 peptide were investigated. To this end, we performed extensive temperature replica exchange molecular dynamics (T-REMD) simulations on Cu^{2+}-bound and unbound α-syn12 peptide using the GROMOS 43A1, OPLS-AA, and AMBER03 force fields. Each replica was run for 300 ns. The structural characteristics of α-syn12 peptide were studied based on backbone dihedral angle distributions, free-energy surfaces obtained with different reaction coordinates, favored conformations, the formation of different Turn structures, and the solvent exposure of the hydrophobic residues. The findings show that AMBER03 prefers to sample helical structures for the unbound α-syn12 peptide and does not sample any β-hairpin structure for the Cu^{2+}-bound α-syn12 peptide. In contrast, the central structure of the major conformational clusters for the Cu^{2+}-bound and unbound α-syn12 peptide according to simulations performed using the GROMOS 43A1 and OPLS-AA force fields is a β-hairpin with $Turn_{9\text{-}6}$. Cu^{2+} can also promote the formation of the β-hairpin and increase the solvent exposure of hydrophobic residues, which promotes the aggregation of α-syn12 peptide. This study can help us to understand the mechanisms through which Cu^{2+} participates in the fibrillation of α-syn12 peptide at the atomic level, which in turn represents a step towards elucidating the nosogenesis of Parkinson's disease.

Keywords Cu^{2+}-bound α-syn12 peptide · Effects of Cu^{2+} · Effects of different force fields · Temperature replica exchange · Free-energy surface · Solvent exposure of hydrophobic residues

Introduction

Parkinson's disease is a degenerative disorder of the central nervous system. A typical symptom of Parkinson's disease is the presence of α-synuclein aggregates in the form of β-structures that can be soluble or insoluble [1, 2]. The N-terminal region of α-synuclein plays a key role in the formation of α-synuclein assemblies [3]. Moreover, many studies have shown that the aggregation of α-synuclein is stimulated by Cu^{2+} under a wide range of concentrations [4, 5]. One interesting question is: which site on α-synuclein does the Cu^{2+} bind to? Although this question has been studied for quite some time [5–9], there is still no consensus on the exact binding site involved in this interaction. Most studies [10–16] have pointed out that the N-terminal region of α-synuclein contains a high-affinity binding site. Unfortunately, it is difficult to experimentally determine and compare the structural characteristics of the Cu^{2+}-bound N-terminal region of α-synuclein with those of the unbound N-terminal region in water.

An alternative way to perform such a comparison is to study the Cu^{2+}-bound N-terminal region of α-synuclein and the unbound N-terminal region in water using molecular

Electronic supplementary material The online version of this article (doi:10.1007/s00894-012-1664-0) contains supplementary material, which is available to authorized users.

Z. Cao · L. Zhao · H. Li · J. Wang
Shandong Provincial Key Laboratory of Functional Macromolecular Biophysics,
Dezhou 253023, China

Z. Cao · L. Zhao · H. Li · J. Wang (✉)
Department of Physics, Dezhou University,
Dezhou 253023, China
e-mail: jhwyh@yahoo.com.cn

L. Liu
Department of Computer Science and Technology,
Dezhou University,
Dezhou 253023, China

dynamics (MD) simulations. Indeed, some researchers have studied the effects of different metal ions on the structural characteristics of other amyloidogenic peptides via MD simulations. For example, Riihimaki et al. investigated the interaction between Cu^{2+} and the octapeptide PHGGGWGQ in the human prion protein by performing molecular dynamics simulations [17]. Miller et al. observed that Zn^{2+} coordinates with Aβ oligomers, decreasing the solvation of the oligomer and promoting Zn^{2+}-Aβ aggregation, in their molecular dynamics simulations [18]. Rose et al. probed the structure of the full-length Cu^{2+}-bound α-synuclein and found that Cu^{2+} causes structural modification at the binding site, leading to a stable turn-like structure [19]. Although those works provided information on how metal ions affect the structural characteristics of amyloidogenic peptides, to our knowledge, there is no report of any comparison of the structural characteristics of Cu^{2+}-bound and unbound α-syn12 peptide in water, as modeled by molecular dynamics simulations with different force fields.

On the other hand, many studies have demonstrated that the quality of molecular dynamic simulations of proteins and peptides depends greatly on the accuracy of the empirical force fields used in them. Matthes et al. [20] presented a systematic study of secondary structure in five peptides modeled using eight different force fields in an explicit solvent model, and the results indicated that AMBER03 [21] has a slight preference for helical over extended β-sheet conformations. Best et al. [22] performed extensive simulations of Ala5 in water using twelve different force fields and found that most of the force fields that are currently used overpopulate the α-region. AMBER03, CHARMM27/cmap [23], OPLS-AA/L [24], and GROMOS 43A1 force fields shows better results than other force fields. Todorova et al. [25] performed a comprehensive comparison of five popular force fields used in the modeling of chain B of insulin and found that CHARMM27 and GROMOS 43A1 delivered the best representation. Piana et al. [26] examined the folding pathways of the villin headpiece using four different force fields, and found that the structure of the native state agreed well with that seen experimentally, but the folding mechanism depended on the choice of force field. The folding and unfolding the designed peptide chignolin depend on the force fields used during modeling, as shown by Petra et al. [27]. The above studies focused on nonamyloidogenic peptides. Since each force field was designed with a specific type of biological system in mind, each has its advantages and disadvantages. It is difficult to select an appropriate force field for particular peptide and protein simulations.

In recent years, amyloidogenic peptides such as Aβ peptide, H1 peptide, and α-syn12 peptide, which are related to several protein conformational diseases (for example Alzheimer's disease, prion-related disorders, Parkinson's disease, etc.), have gained a great deal of attention. However, the effects of applying different force fields when modeling amyloidogenic peptides have barely been addressed. Nguyen et al. [28] investigated the effects of three different force fields on $Aβ_{16-22}$ assembly. The results indicated that the AMBER99 force field is not suitable for exploring amyloid formation because of its strong bias towards α-helical structures, the GROMOS 43A1 force field favors a very high population with extended β-sheet structures, and OPLS-AA produces results that are intermediate between those of AMBER99 and GROMOS 43A1. It is difficult to say which of GROMOS 43A1 and OPLS-AA is the most well suited to studying amyloid formation. Cao et al. [29, 30] compared the effects of different force fields on the dynamic and thermodynamic characteristics of H1 peptide (residues 109–122 of the Syrian hamster PrP) in aqueous solution, and the results indicated that the GROMOS 43A1 force field prefers a β-hairpin conformation while the OPLS-AA force field prefers a β-turn conformation. For the peptide $Aβ_{12-28}$, the mostly densely populated conformational state is a random coil when either the GROMOS 43A1 or OPLS-AA force field is used [31]. However, to our best knowledge, there is no report of the effects of using different force fields in long-timescale molecular dynamics simulations of Cu^{2+}-bound and unbound α-syn12 peptide.

Therefore, in the work described in this paper, we compared the structural characteristics of Cu^{2+}-bound and unbound α-syn12 peptide in explicit water at atomic resolution by performing six independent long-timescale temperature replica exchange molecular dynamics (T-REMD) simulations with three different force fields. Thirty-six replicas were used for each simulation, and each replica was simulated for 300 ns. The last 100 ns of each trajectory at 300 K was analyzed. The total molecular dynamics simulation time was 64.8 μs. Structural characteristics were analyzed based on parameters such as backbone dihedral angle distributions, the free-energy surface, the formation of turns, and favored conformations. Overall, these extensive simulations showed that the use of the GROMOS 43A1 and OPLS-AA force fields yielded similar lowest free-energy conformations for the Cu^{2+}-bound and unbound α-syn12 peptide. In contrast, employing the AMBER03 force field produced different structural characteristics, leading to a bias toward a helical structure. The results also indicated that Cu^{2+} modulates the conformational distribution of α-syn12 peptide from a wide conformational space to a narrow one.

Methods

We investigated Cu^{2+}-bound and unbound α-syn12 peptide (residues 1–12 of the human α-synuclein protein; sequence: MDVFMKGLSKAK) in this study. The 2N2O binding

model was chosen; the binding site contained Met-1 amino, Asp-2 backbone amide, and Asp-2 carboxylate groups as well as a water molecule. The bond lengths were assigned according to the calculation reported in the work of Binolfi et al. [11]: the values were 2.056 Å, 1.924 Å, 2.009 Å, and 2.089 Å, respectively. In all of the Cu^{2+}-bound simulations, only one Cu^{2+} was bound at the binding site, and LINCS [32] was used to fix the lengths of the four Cu^{2+}–ligand bonds. The initial structures employed are shown in the "Electronic supplementary material."

MD simulation was performed in the isothermal-isobaric (NPT) ensemble using the GROMACS software package [33]. Three different simulation models were considered: (1) the GROMOS 43A1 [34] force field with the SPC [35] water model; (2) the OPLS-AA [24] force field with the TIP3P [36] water model; (3) the AMBER03 [21] force field with the TIP3P water model. The peptide was solvated in a rectangular box with the minimum distance from the solute to the boundary of the box set to 1.0 nm. The simulated systems for the three different force fields contained 1710, 1851, and 1855 water molecules, respectively. Long-range electrostatic interactions were treated using the particle-mesh Ewald method, with a grid spacing of 0.12 nm and fourth-order interpolation [37, 38]. The protonation states of ionizable groups were assigned to be those present at pH 7.0. For the unbound α-syn12 peptide, two negative counterions (Cl^-) were added to produce a neutral simulation system. For the Cu^{2+}-bound α-syn12 peptide, four negative counterions (Cl^-) were added to produce a neutral simulation system.

The temperature of the system was kept constant using velocity rescaling with a stochastic term [39]. The pressure (set to 1 atm) of the system was kept constant using a weak coupling algorithm [40]. Simulation was performed using a temperature coupling time of 0.1 ps, a pressure coupling time of 0.5 ps, and an isothermal compressibility of 4.575×10^{-4} $(kJ\,mol^{-1}\,nm^{-3})^{-1}$. The time step for the MD integrator was set to 2 fs, and LINCS [32] was applied to constrain all bond lengths.

The six independent T-REMD [41] simulations were performed starting from the Cu^{2+}-bound and unbound α-syn12 peptide [the initial α-helix conformation was selected from the NMR-determined micelle-bound structure at neutral pH (PDB ID: 1XQ8)] and using three different force fields. Each independent T-REMD had 36 replicas that were simulated at temperatures (in K) of 273, 275, 278, 280, 283, 285, 288, 290, 293, 295, 298, 300, 303, 306, 309, 312, 314, 317, 320, 322, 325, 328, 331, 334, 337, 340, 343, 345, 348, 351, 354, 357, 360, 363, 367, and 370 [42]. Effective T-REMD requires sufficient exchange between the different temperatures (the exchange ratio is greater than 0.1). The exchange ratios were between 35 % and 46 % in these simulations, so the number of replicas was sufficient. Each replica was equilibrated at its respective temperature for 100 ps. Three-hundred-nanosecond T-REMD simulations were then performed, with replica exchanges attempted every 2 ps according to the Metropolis criterion. Coordinates and energies were recorded every 2 ps. The last 100 ns of each trajectory at 300 K was analyzed. It should be noted that the convergence of conformational sampling starting from an α-helix was verified by performing simulations starting from an irregular structure, as in our previous work [43].

Results and discussion

Effects of Cu^{2+} binding and the use of different force fields during modeling on the backbone dihedral angle distributions

In order to evaluate the influence of Cu^{2+} binding and the use of different force fields during modeling on the backbone conformations of the α-syn12 peptide, we analyzed the backbone (φ, ψ) angle distributions for residues 2–11. The data for these residues were pooled. The dihedral (φ, ψ) angles of each residue were collected from the simulations, and potentials of mean force were computed (see Fig. 1).

The distributions sampled by simulations of the Cu^{2+}-bound and unbound α-syn12 peptide using the three force fields were, in general, quite different from each other. Various regions of the distributions were defined as in [44]; i.e., α region: $-180° < \varphi < 0°$ and $-120° < \psi < 30°$, bridge region: $-180° < \varphi < 0°$ and $30° < \psi < 90°$, β region: $-180° < \varphi < 0°$ and $90° < \psi < 180°$ or $-180° < \psi < -120°$. For the GROMOS 43A1 force field, the probabilities that the (φ, ψ) angles fall into the α region were 11 % and 20 % for the Cu^{2+}-bound and unbound α-syn12 peptide, respectively, while the probabilities that they fall into the β region were 66 % and 58 %. For the OPLS-AA force field, the probabilities that the (φ, ψ) angles fall into the α region were 13 % and 21 % for the Cu^{2+}-bound and unbound α-syn12 peptide, respectively, while probabilities that they fall into the β region were 70 % and 61 %. For the AMBER03 force field, the probabilities that the (φ, ψ) angles fall into the α region were 44 % and 78 % for the Cu^{2+}-bound and unbound α-syn12 peptide, respectively, while the probabilities that the (φ, ψ) angles fall into the β region were 44 % and 16 % (details are listed in Table 1). The AMBER03 force field shows a strong bias towards α-helical structures compared with the OPLS-AA and GROMOS 43A1 force fields, which is consistent with the results of other simulations of nonamyloidogenic peptides [20, 45]. Moreover, Cu^{2+} can promote the conformational transitions from the α region to the β region when modeling using any of the three force fields.

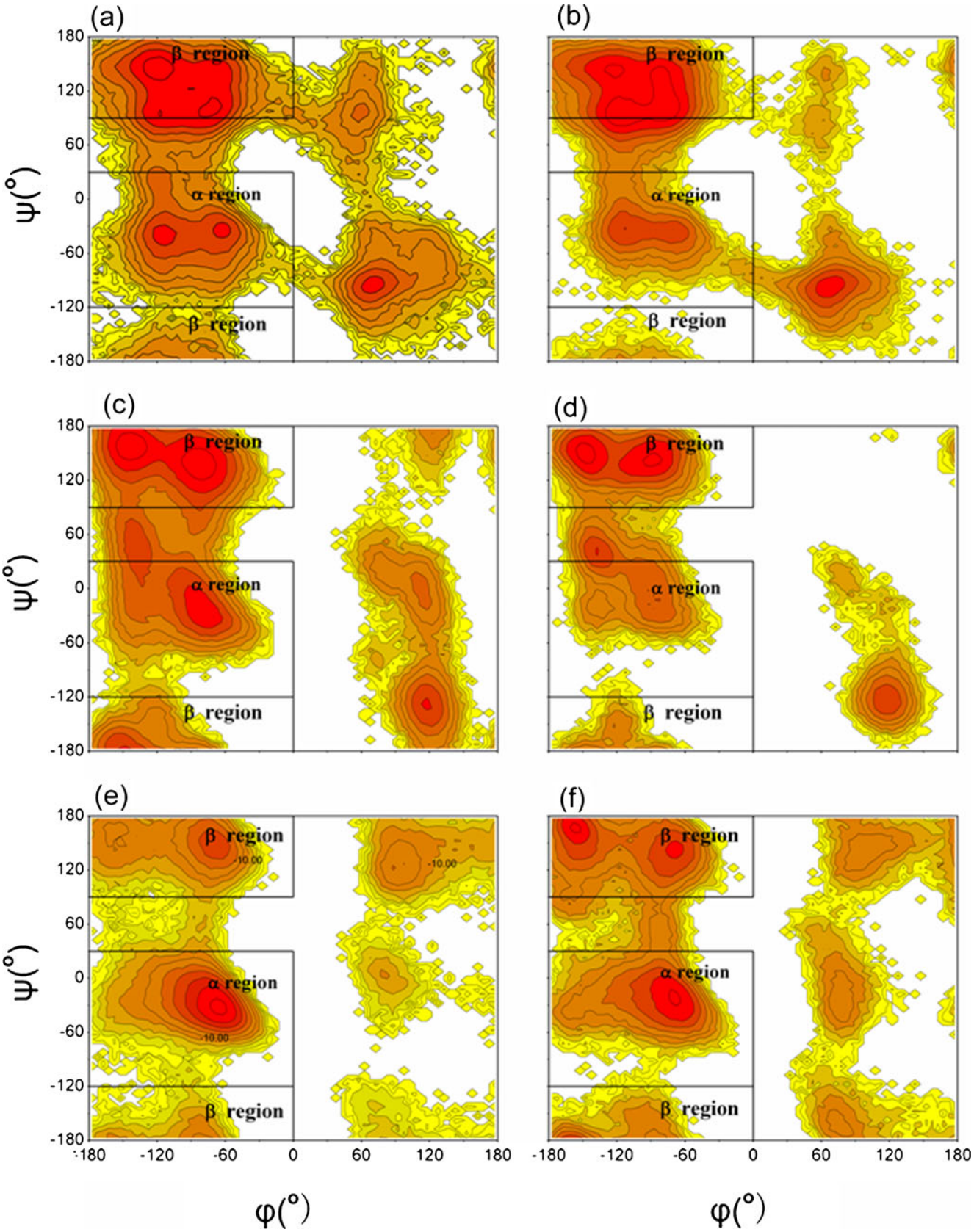
(a)
(b)
(c)
(d)
(e)
(f)
β region
α region
β region
ψ(°)
φ(°)
180
120
60
0
-60
-120
-180
-10.00

◀ **Fig. 1a–f** Potentials of mean force plotted as a function of the Ramachandran (φ, ψ) angles for residues 2–11 in simulations of **a** the unbound α-syn12 peptide using the GROMOS 43A1 force field, **b** the Cu^{2+}-bound α-syn12 peptide using the GROMOS 43A1 force field, **c** the unbound α-syn12 peptide using the OPLS-AA force field, **d** the Cu^{2+}-bound α-syn12 peptide using the OPLS-AA force field, **e** the unbound α-syn12 peptide using the AMBER03 force field, **f** the Cu^{2+}-bound α-syn12 peptide using the AMBER03 force field. Neighboring contour lines are separated by 2 $kJmol^{-1}$

The fact that Cu^{2+} promotes transitions can also be seen in the relative depths of the β, $P_{II,}$ and α_R minima. For the GROMOS 43A1 force field, the relative depths were 0.0, 0.7, and 2.5 $kJmol^{-1}$ for the unbound α-syn12 peptide, whereas the corresponding depths were 0.0, 0.0, and 3.4 $kJmol^{-1}$ for the Cu^{2+}-bound α-syn12 peptide. For the OPLS-AA force field, the relative depths were 0.0, 0.4, and 2.1 $kJmol^{-1}$ for the unbound α-syn12 peptide, while the corresponding depths were 0.0, 0.4, and 4.7 $kJmol^{-1}$ for the Cu^{2+}-bound α-syn12 peptide. For the AMBER03 force field, the relative depths were 0.0, −4.8, and −9.8 $kJmol^{-1}$ for the unbound α-syn12 peptide, while the corresponding depths were 0.0, 1.9, and 0.2 $kJmol^{-1}$ for the Cu^{2+}-bound α-syn12 peptide (details are listed in Table 2). For the GROMOS 43A1 and OPLS-AA force fields, the β region was always the lowest minimum, and Cu^{2+} was able to enlarge the free-energy gap between the β region and the α region.

Residue-specific secondary structure propensity

Figure 1 shows that the simulations sampled the three different regions for the six simulations. However, it is difficult to identify the type of secondary structure associated with each residue based on the probabilities of the backbone (φ, ψ) angles. The residue-specific secondary structure propensity of α-syn12 peptide was calculated with the program STRIDE [46]. The results of our analysis of all 12 residues when modeling is performed using the three different force fields are shown in Fig. 2. The program STRIDE distinguishes seven different types of secondary structure: α-helix, 3_{10} helix, π helix, extended conformation, isolated bridge, turn, and random coil.

It is clear from Fig. 2 that the AMBER03 force field yields different results than the other two force fields. The main differences are as follows. First, in the simulations with the GROMOS 43A1 and OPLS-AA force fields, the α-helix and 3_{10} helix populations vanish, whereas the α-helix population comprises about 60 % of the total population when the AMBER03 force field is used. Second, a large β-strand population is observed for residues F4-K6 and S9-A11 (larger than 35 % of the total population) when the GROMOS 43A1 and OPLS-AA force fields are used. These two β-strand regions are connected by $Turn_{9\text{-}6}$ (i.e., a β-turn at residues 6–9). The formation of β-turns and β-hairpins were estimated by the program STRIDE. However, simulation with the AMBER03 force field shows no obvious tendency to form β-strands.

Table 1 Probabilities that the (φ, ψ) angles fall within different regions for the Cu^{2+}-bound and unbound α-syn12 peptide modeled using three force fields (data for the unbound α-syn12 peptide are given in parentheses)

	GROMOS 43A1	OPLS-AA	AMBER03
α Region	0.11 (0.20)	0.13 (0.21)	0.44 (0.78)
Bridge region	0.13 (0.09)	0.08 (0.07)	0.03 (0.00)
β Region	0.66 (0.58)	0.70 (0.61)	0.44 (0.16)

Table 2 Relative depths of the free-energy minima of α-syn12 peptide (modeled using different force fields) in Ramachandran (φ, ψ) angle distributions (the data for the unbound α-syn12 peptide are given in parentheses)

	Relative depth ($kJmol^{-1}$) of the minimum		
Force field	GROMOS 43A1	OPLS-AA	AMBER03
β	0.0 (0.0)	0.0 (0.0)	0.0 (0.0)
P_{II}	0.0 (0.7)	0.4 (0.4)	1.9 (−4.8)
α_R	3.4 (2.5)	4.7 (2.1)	0.2 (−9.8)

All conformational clusters based on $RMSD_{C\alpha}$

The above results show that the main secondary structures derived from simulations performed using the GROMOS 43A1 and OPLS-AA force fields are quite different from those derived from simulations performed using the AMBER03 force field. It is very important to obtain and compare the favored conformations yielded by the different force fields. One way to identify the favored conformations of the unbound and the Cu^{2+}-bound α-syn12 peptide in solution is to cluster all of the conformations based on the root-mean-square deviations in the positions of Cα atoms ($RMSD_{C\alpha}$). For the six independent simulations, we chose to analyze the conformations of the 300 K replica. A total of 50,000 conformations obtained during the last 100 ns of each trajectory were clustered based on their pair-wise $RMSD_{C\alpha}$ values. Conformations were assumed to be in the same cluster when the $RMSD_{C\alpha}$ among the conformations was <0.1 nm. When these clustering criteria were applied, the conformations observed in the simulations fell into clusters of different sizes.

In order to analyze simulation convergence, the populations of the conformational clusters were calculated. The results are shown in Fig. 3. Here, the overall 100 ns of the trajectory analyzed is divided into two 50 ns blocks. Only clusters that contained at least 3 % of all conformations were selected and counted as a function of time. The results show

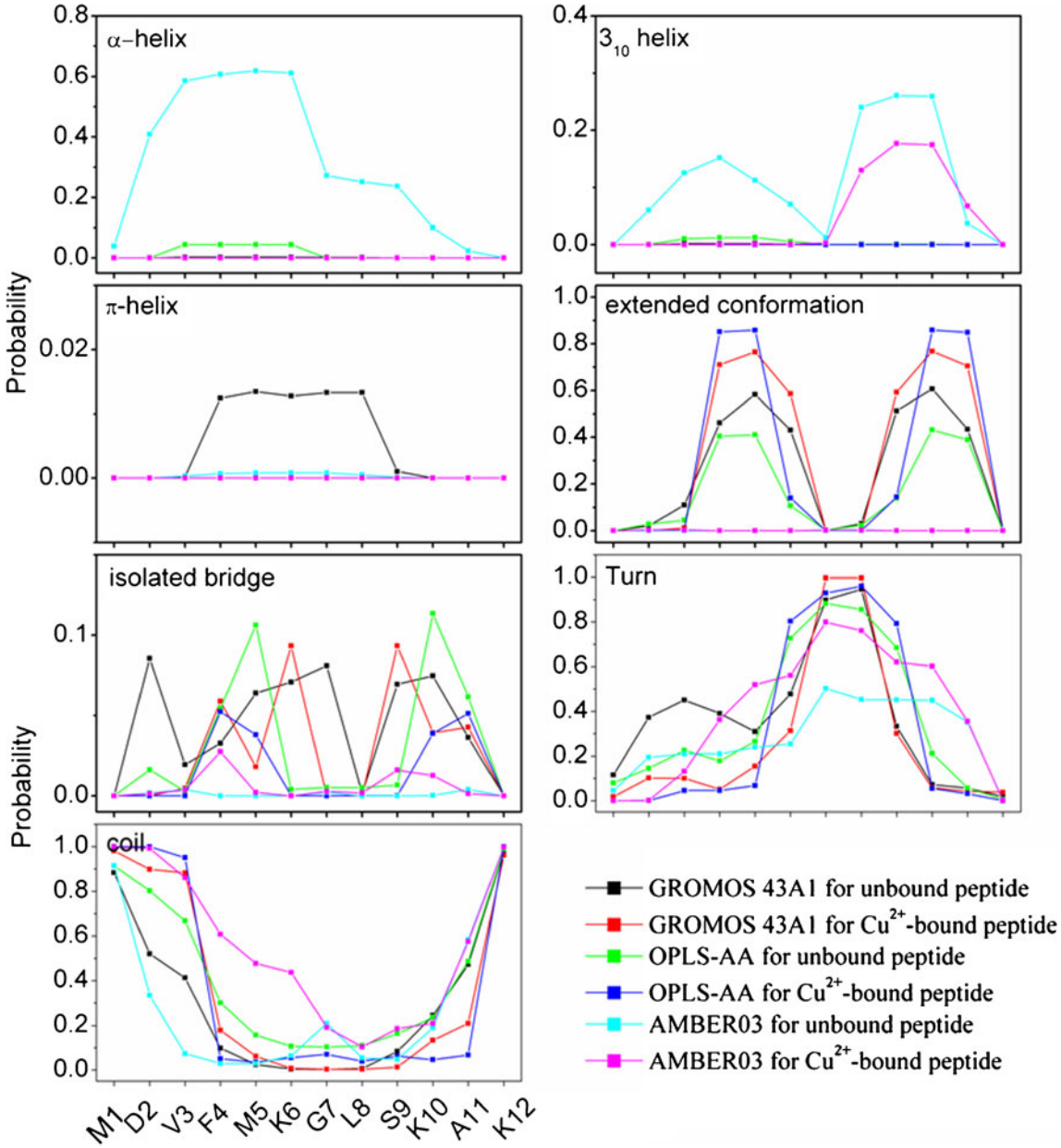

Fig. 2 Residue-specific secondary structure propensities of α-syn12 peptide modeled using different force fields. The STRIDE protocol distinguishes seven different types of secondary structure

that 300 ns of simulation are enough to achieve system convergence.

When the GROMOS 43A1 force field was used, the representative structure for the unbound α-syn12 peptide was a β-hairpin with $Turn_{9\text{-}6}$ and three hydrogen bonds ($HB_{4\text{-}11}$, $HB_{6\text{-}9}$, and $HB_{11\text{-}4}$); this cluster contained 42 % of all the conformations. The representative structure for the Cu^{2+}-bound α-syn12 peptide was a β-hairpin with $Turn_{9\text{-}6}$ and four hydrogen bonds ($HB_{4\text{-}11}$, $HB_{6\text{-}9}$, $HB_{9\text{-}6}$, and $HB_{11\text{-}4}$); this cluster contained 99 % of all the conformations. When the OPLS-AA force field was used, the representative structure for unbound α-syn12 peptide was a β-hairpin with $Turn_{9\text{-}6}$ and three hydrogen bonds ($HB_{4\text{-}11}$, $HB_{6\text{-}9}$, and $HB_{11\text{-}4}$); this cluster contained 51 % of all the conformations. The representative structure for the Cu^{2+}-bound α-syn12 peptide was a β-hairpin with $Turn_{9\text{-}6}$ and two hydrogen bonds ($HB_{6\text{-}9}$ and $HB_{11\text{-}4}$); this cluster contained 94 % of all the conformations. When the AMBER03 force field was used, the largest cluster for unbound α-syn12 peptide contained 76 % of the conformations, and the representative structure of this cluster was a helical structure with an α-helix for residues 2–6 and a 3_{10} helix for residues 8–10; the representative structure for the Cu^{2+}-bound α-syn12

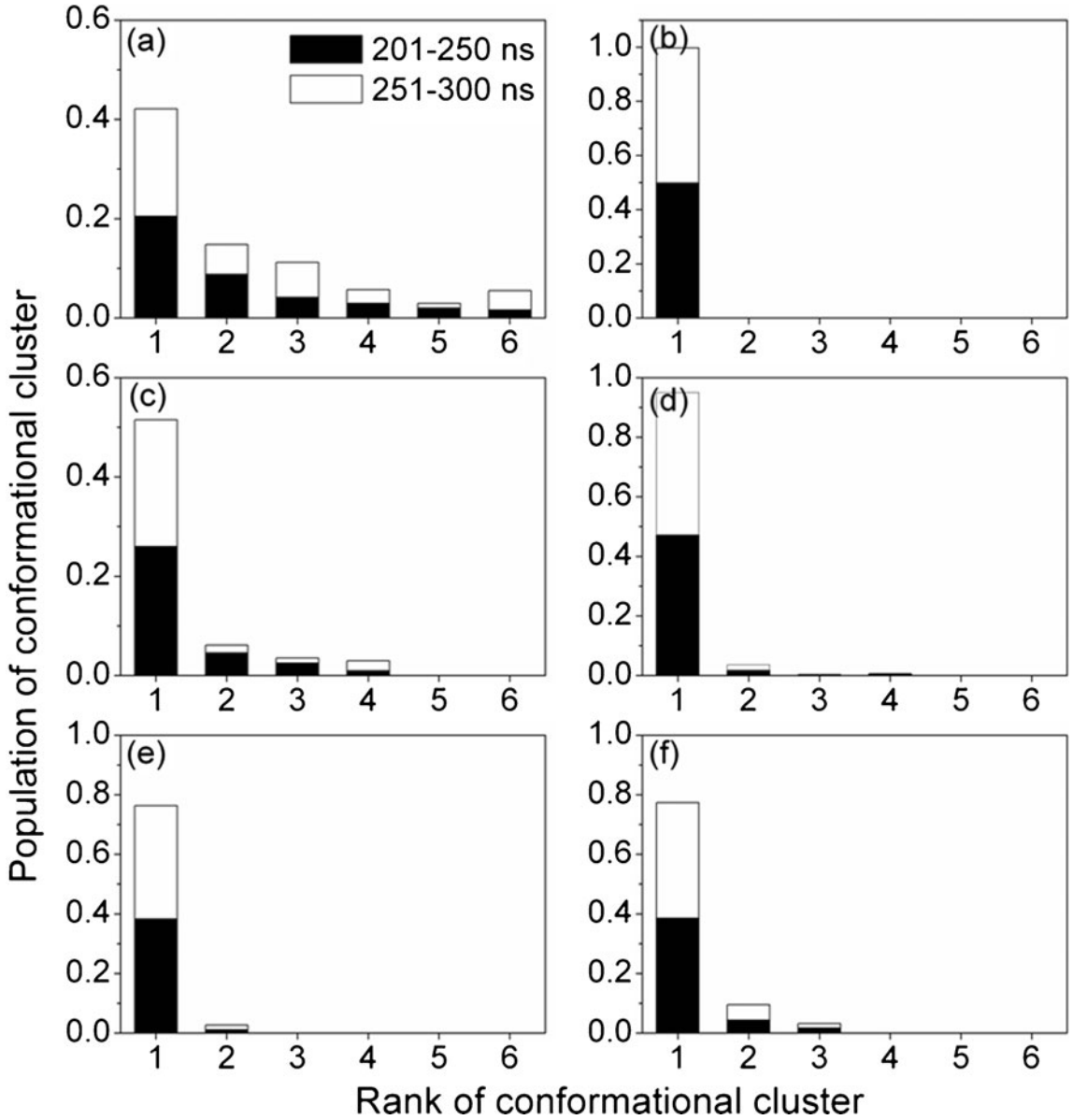

Fig. 3a–f Conformational clustering analysis for **a** unbound α-syn12 peptide modeled using the GROMOS 43A1 force field, **b** Cu^{2+}-bound α-syn12 peptide modeled using the GROMOS 43A1 force field, **c** unbound α-syn12 peptide modeled using the OPLS-AA force field, **d** Cu^{2+}-bound α-syn12 peptide modeled using the OPLS-AA force field, **e** unbound α-syn12 peptide modeled using the AMBER03 force field, **f** Cu^{2+}-bound α-syn12 peptide modeled using the AMBER03 force field. The populations of the conformational clusters are shown in decreasing order. *Black bars* represent the simulation period 201–250 ns, *white bars* represent 251–300 ns

peptide was a coil structure. The favored conformations sampled by simulations of the Cu^{2+}-bound and unbound α-syn12 peptide using the GROMOS 43A1 and OPLS-AA force fields were, in general, quite similar to each other. However, the AMBER03 force field preferred to sample α-helical structure. Moreover, Cu^{2+} promoted the formation of a β-hairpin conformation with $Turn_{9\text{-}6}$ when using the GROMOS 43A1 and OPLS-AA force fields and suppressed the formation of an α-helical conformation when the AMBER03 force field was used.

Root mean square deviations of C_α atoms ($RMSDC_\alpha$)

The root mean square deviations (RMSD) of the positions of C_α atoms with respect to the positions of those atoms in the representative structure derived from the conformational clusters obtained in the Cu^{2+}-bound α-syn12 peptide simulations are plotted in Fig. 4 as a function of the simulation time. The $RMSDC_\alpha$ distributions are also shown. The final 100 ns of each trajectory was divided into two 50 ns blocks to calculate the distributions. The results show that a 300 ns simulation is sufficiently long to allow the system to converge.

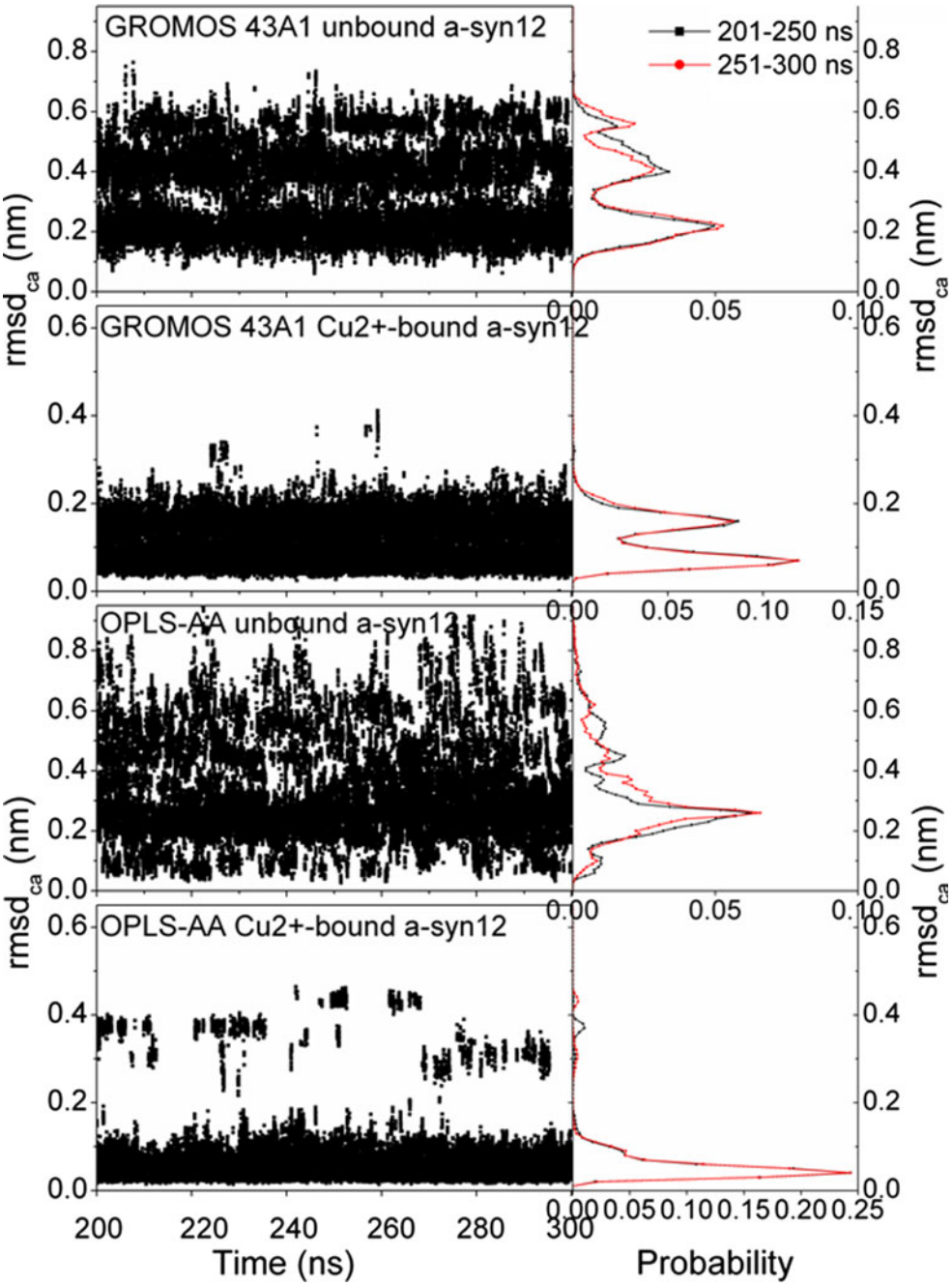

Fig. 4 Temporal evolutions (*left panels*) and distributions (*right panels*) of the root mean square deviations of the positions of alpha-carbon atoms with respect to the positions of those atoms in the representative structure derived from the conformational clusters obtained in the Cu^{2+}-bound α-syn12 peptide simulations

Free-energy surfaces based on different reaction coordinates

Another simple and widely used method of representing the conformational space of a peptide visually is to construct free-energy surfaces (FESs) based on two reaction coordinates. According to the above analysis, the favored conformation when using the GROMOS 43A1 and OPLS-AA force fields is a β-hairpin with $Turn_{9\text{-}6}$. In this conformation, not only is a turn present, but also the termini are in close proximity: the distance between F4(H) and A11(O) is less than 0.3 nm. Therefore, we chose the distance between F4 (H) and A11(O) as well as the root mean square deviations of the positions of C_α atoms ($RMSDC_\alpha$) from the positions of those atoms in the representative structure derived from the conformational clusters obtained in the Cu^{2+}-bound α-syn12 peptide simulations as the reaction coordinates. The corresponding FESs (see Fig. 5) indicate that the conformations with the lowest minima in two-dimensional space exhibited a β-hairpin.

For the Cu^{2+}-bound α-syn12 peptide, the GROMOS 43A1 force field sampled two minima centered near (0.23 nm, 0.07 nm) and (0.58 nm, 0.15 nm) with relative depths of 0.0 and 4.2 $kJ\,mol^{-1}$, whereas the OPLS-AA force field sampled two minima centered near (0.30 nm, 0.05 nm)

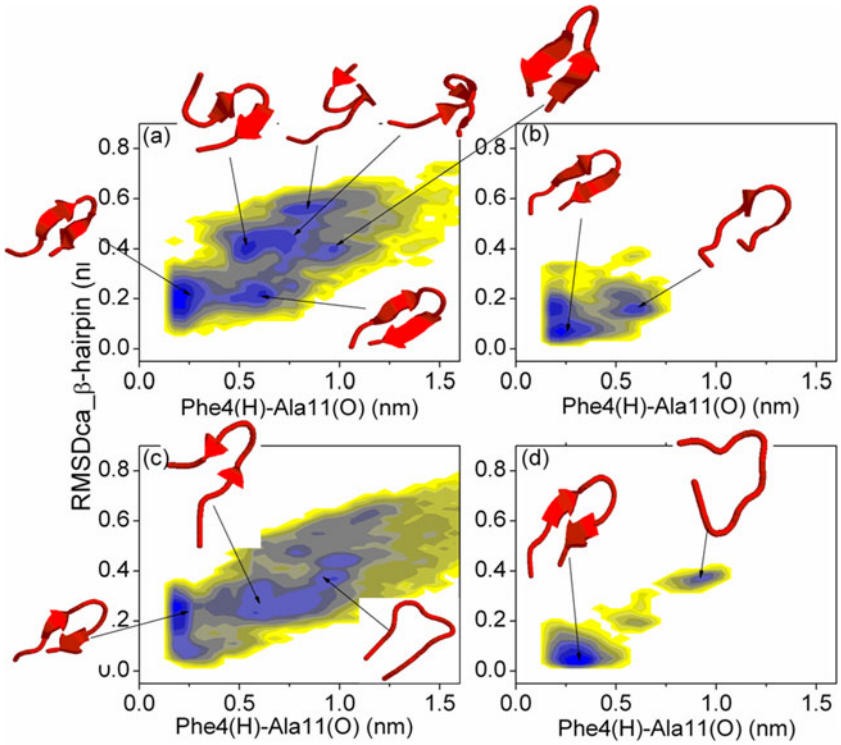

Fig. 5a–d Free-energy surfaces constructed according to the distance between F4(H) and A11 (O) and the root mean square deviations (RMSD) of the positions of C_α atoms the positions of those atoms in the representative structure derived from the conformational clusters obtained in the Cu^{2+}-bound α-syn12 peptide simulations. **a** Unbound α-syn12 peptide modeled using the GROMOS 43A1 force field, **b** Cu^{2+}-bound α-syn12 peptide modeled using the GROMOS 43A1 force field, **c** unbound α-syn12 peptide modeled using the OPLS-AA force field, **d** Cu^{2+}-bound α-syn12 peptide modeled using the OPLS-AA force field. Neighboring contour lines are separated by 1 $kJmol^{-1}$. The representative structures are shown in *red*

and (0.92 nm, 0.37 nm) with relative depths of 0.0 and 6.4 $kJmol^{-1}$. These results again show that the sampling for the Cu^{2+}-bound α-syn12 peptide focused on the regions corresponding to a β-hairpin conformation.

For the unbound α-syn12 peptide, the GROMOS 43A1 force field sampled six minima centered near (0.23 nm, 0.21 nm), (0.53 nm, 0.39 nm), (0.63 nm, 0.21 nm), (0.78 nm, 0.55 nm), (0.72 nm, 0.43 nm), and (0.97 nm, 0.39 nm), with relative depths of 0.0, 2.2, 2.5, 3.3, 3.4, and 4.7 $kJmol^{-1}$, whereas the OPLS-AA force field sampled three minima centered near (0.18 nm, 0.25 nm), (0.98 nm, 0.37 nm), and (0.58 nm, 0.23 nm), with relative depths of 0.0, 4.3, and 4.8 $kJmol^{-1}$. These results indicate that the sampling for the unbound α-syn12 peptide was diverse, and are consistent with the results obtained from the conformational clusters.

The representative structures for each minimum are presented in Fig. 5. The lowest free-energy conformations were similar for simulations performed with the GROMOS 43A1 and OPLS-AA force fields. However, the conformations for the local minima are quite different from each other. The unbound α-syn12 peptide prefers to form conformations with both $Turn_{5\text{-}2}$ and $Turn_{9\text{-}6}$. A more detailed analysis is shown in the "Turn formation" section.

Another widely used method of constructing the free-energy surfaces (FESs) is to two principal components (PC1 and PC2) as the reaction coordinates (see Fig. 6). Therefore, we performed principal components analysis (PCA) using the programs "g_covar" and "g_anaeig" in the GROMACS package [47]. In the PCA, only the fluctuations of all of the backbone atoms of this peptide were used. The two principal components from PCA were used as reaction coordinates to describe the free-energy surfaces at 300 K (see Fig. 6). For the unbound α-syn12 peptide, the simulations invariably sampled a wide variety of conformational states. However, the simulations for the Cu^{2+}-bound α-syn12 peptide sampled just one conformational state: Cu^{2+} binding drastically reduces the size of the conformational space of the α-syn12 peptide. The corresponding representative structures are shown in Fig. 6. For the simulations performed using the GROMOS 43A1 and OPLS-AA force fields, there was only a marginal difference between the representative structures of the unbound and the Cu^{2+}-bound α-syn12 peptide, which was a β-hairpin with $Turn_{9\text{-}6}$. However, for the simulations performed with the AMBER03 force field, there was a much larger difference between the representative structures of the unbound and the Cu^{2+}-bound α-syn12 peptide. The unbound α-syn12 peptide, preferred to form an α-helix, whereas the Cu^{2+}-bound α-syn12 peptide prefered to form a coiled structure.

Turn formation

β-Hairpin configurations were produced in the simulations of both the unbound and the Cu^{2+}-bound α-syn12 peptide modeled using the GROMOS 43A1 and OPLS-AA force fields. Furthermore, the β-turn is one of the most important influences on β-hairpin stability. Figure 2 indicates that the

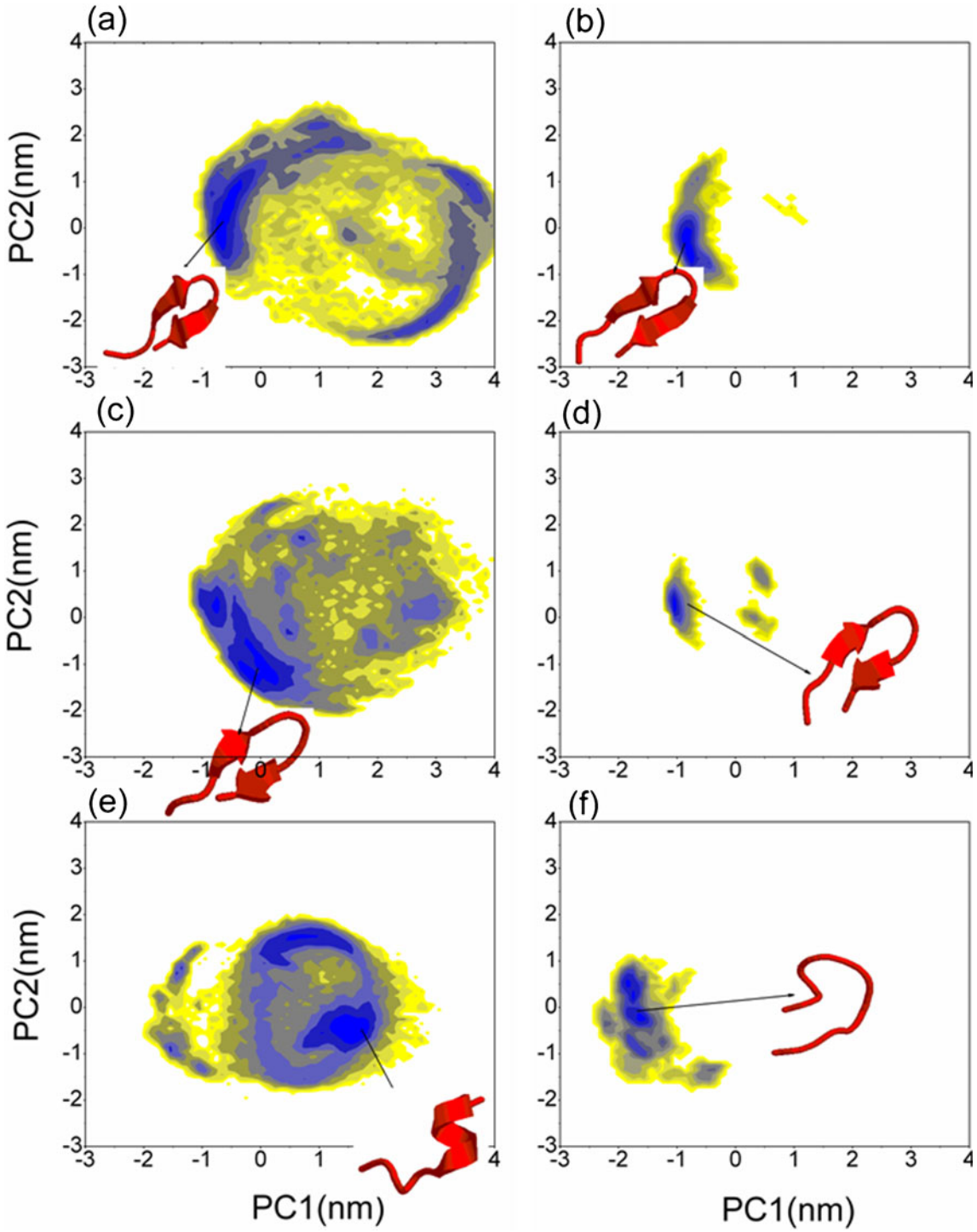

Fig. 6a–f Free-energy surfaces plotted using the first two principal components (PC-1 and PC-2) as reaction coordinates for simulations of **a** the unbound α-syn12 peptide modeled using the GROMOS 43A1 force field, **b** the Cu^{2+}-bound α-syn12 peptide modeled using the GROMOS 43A1 force field, **c** the unbound α-syn12 peptide modeled using the OPLS-AA force field, **d** the Cu^{2+}-bound α-syn12 peptide modeled using the OPLS-AA force field, **e** the unbound α-syn12 peptide modeled using the AMBER03 force field, and **f** the Cu^{2+}-bound α-syn12 peptide modeled using the AMBER03 force field. Neighboring contour lines are separated by 2 $kJmol^{-1}$. The representative structures are shown in *red*

conformational space sampled in simulations of the Cu^{2+}-bound α-syn12 peptide is significantly smaller than that sampled in the simulations of unbound α-syn12 peptide. Figure 5 indicates that the properties of the state corresponding to the local minimum differ significantly for different force fields. The simulation results depend which force field is used, which

is consistent with the results observed for other simulations [26]. In order to investigate the influence of Cu^{2+} and different force fields on the secondary structure of the α-syn12 peptide, we analyzed the probabilities of forming different β-turns when modeling using different force fields (see Fig. 7). For unbound α-syn12 peptide, the respective probabilities that the conformation has $Turn_{9\text{-}6}$ were 85 %, 65 %, and 5 % for the GROMOS 43A1, OPLS-AA, and AMBER03 force fields, respectively. However, for the Cu^{2+}-bound α-syn12 peptide, the respective probabilities that the conformation has $Turn_{9\text{-}6}$ were 98 %, 88 %, and 8 % for the three different force fields. These results indicate that the binding of Cu^{2+} can promote the formation of $Turn_{9\text{-}6}$ and suppress the formation of other turns. The unbound α-syn12 peptide preferred to form conformations with $Turn_{5\text{-}2}$ when the GROMOS 43A1 force field was used.

In order to further analyze the structural features of the Cu^{2+}-bound and unbound α-syn12 peptide, we divided the conformations into six different "states:" (1) forms $Turn_{5\text{-}2}$ but does not form $Turn_{9\text{-}6}$, and the distance between F4(H) and A11(O) is <0.3 nm; (2) forms $Turn_{5\text{-}2}$ but does not form $Turn_{9\text{-}6}$, and the distance between F4(H) and A11(O) is ≥0.3 nm; (3) forms $Turn_{9\text{-}6}$ but do not form $Turn_{5\text{-}2}$, and the distance between F4(H) and A11(O) is <0.3 nm; (4) forms $Turn_{9\text{-}6}$ but does not form $Turn_{5\text{-}2}$, and the distance between F4(H) and A11(O) is ≥0.3 nm; (5) forms both $Turn_{9\text{-}6}$ and $Turn_{5\text{-}2}$, and the distance between F4(H) and A11(O) is <0.3 nm; (6) forms both $Turn_{9\text{-}6}$ and $Turn_{5\text{-}2}$, and the distance between F4(H) and A11(O) is ≥0.3 nm. The respective probabilities that conformations for the Cu^{2+}-bound and unbound α-syn12 peptide occur in each state when each of the force fields is used are summarized in Table 3. The table shows that the Cu^{2+}-bound α-syn12 peptide is unlikely to form $Turn_{5\text{-}2}$. However, the unbound α-syn12 peptide is inclined to form $Turn_{5\text{-}2}$. It is likely that the Cu^{2+}-bound α-syn12 peptide only forms $Turn_{9\text{-}6}$ because there is electrostatic repulsion between Asp2 (the binding site of Cu^{2+} contains Asp2, which causes Asp2 to have a positive charge) and Lys6.

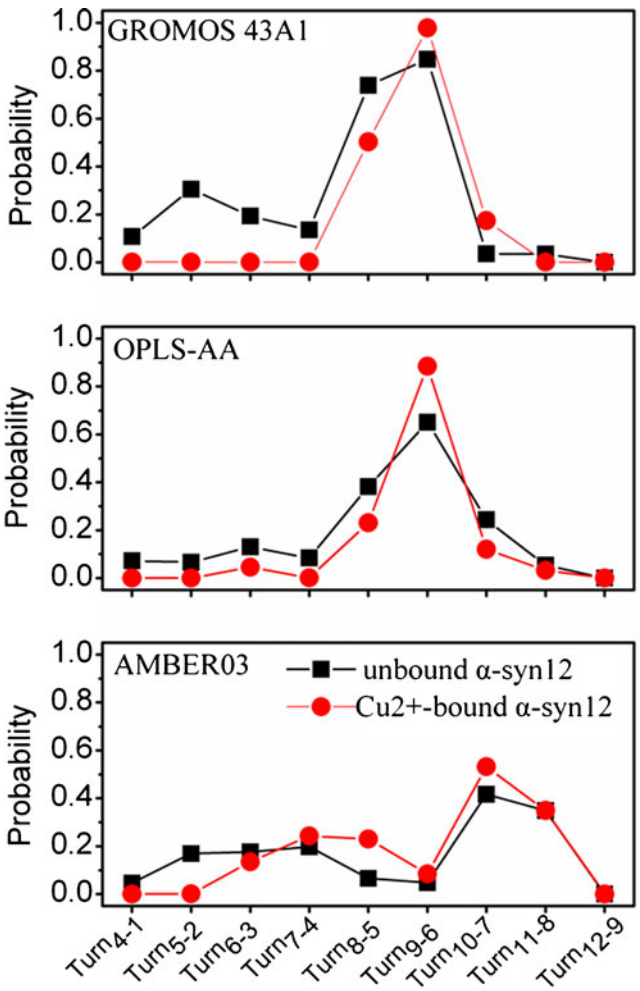

Fig. 7 The probability that a particular type of β-turn is formed when a particular force field is employed during modeling

Solvent exposure of the hydrophobic residues

Because the interactions of solvent-exposed hydrophobic residues represent a major driving force for protein aggregation [48], we calculated the distribution of solvent exposure for all of the hydrophobic residues (S_{pho}; the residues Met1, Val3, Phe4, Met5, Leu8, and Ala11 were considered hydrophobic residues), the solvent exposure of all residues (S_{all}), as well as the fraction (f_{pho}) of the solvent-accessible surface that corresponds to S_{pho} ($f_{pho}=S_{pho}/S_{all}$; see Fig. 8).

The simulations of the Cu^{2+}-bound α-syn12 peptide prefer to sample conformations characterized by relatively high solvent exposure of the hydrophobic residues and all residues. These increases of solvent exposure of the hydrophobic residues and all residues are in different degrees which induce the simulations for the Cu^{2+}-bound α-syn12 peptides prefer to sample conformation with larger f_{pho} than simulations for unbound α-syn12 peptide. These results show why Cu^{2+} promotes the aggregation of α-synuclein protein.

Asp2 is in the binding site of Cu^{2+}, which leads to electrostatic repulsion between Asp2 and Lys6 (the two residues carry positive charges). As a result, the Cu^{2+}-bound α-syn12 peptide only forms $Turn_{9\text{-}6}$, and the interactions between the first five

Table 3 The respective probabilities that conformations will occur in six different states when modeling Cu^{2+}-bound and unbound α-syn12 peptide using three force fields (the data for the unbound α-syn12 peptide are given in parentheses)

	GROMOS 43A1	OPLS-AA	AMBER03
State 1	0 (0)	0 (0)	0 (0)
State 2	0 (0.08)	0 (0.05)	0 (0.16)
State 3	0.76 (0.31)	0.38 (0.35)	0 (0)
State 4	0.22 (0.31)	0.50 (0.29)	0.08 (0.04)
State 5	0 (0)	0 (0)	0 (0)
State 6	0 (0.22)	0 (0.01)	0 (0.01)

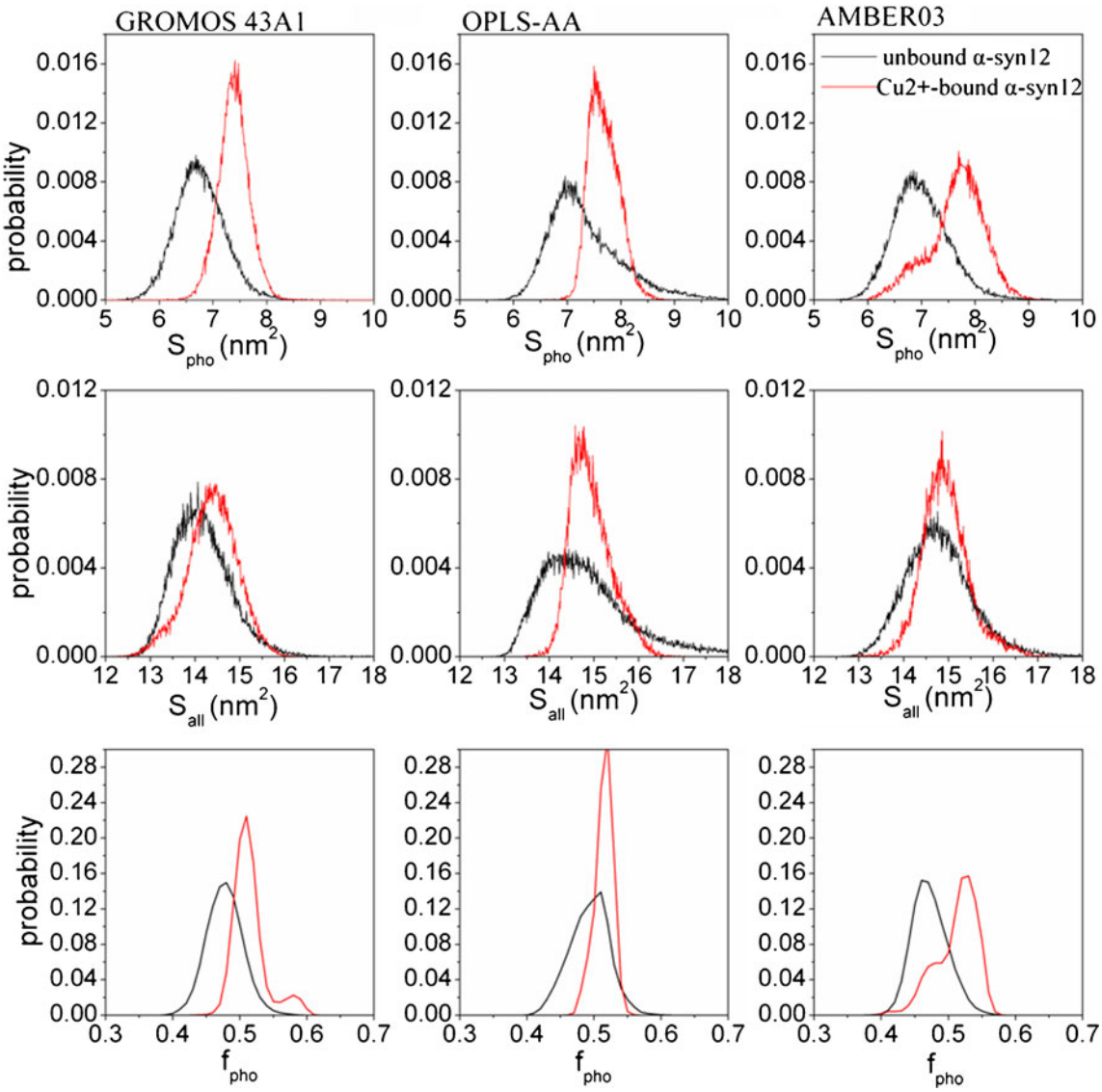

Fig. 8 The distribution of solvent exposure for the hydrophobic residues (S_{pho}; *first row*), the solvent exposure of all residues (S_{all}; *second row*), and the fraction of the solvent-accessible surface that corresponds to S_{pho} (f_{pho}; *third row*)

residues and water are enhanced. This hypothesis is validated by calculations of f_{pho} for residues 1, 3, 4, and 5 and f_{pho} for residues 8 and 11 (see Fig. 9). The results show that Cu^{2+} increases the solvent exposure of hydrophobic residues 1, 3, 4, and 5. This conclusion hints at why Cu^{2+} promotes the aggregation of α-syn12 peptide. The increased solvent exposure of hydrophobic residues 1, 3, 4, and 5 enhances hydrophobic interactions between the hydrophobic residues from different peptides.

Conclusions

Molecular dynamics simulation is a valid method for investigating structural characteristics that are difficult to study experimentally. Generally, the quality of a molecular dynamic simulation of a protein or peptide depends greatly on the accuracy of the empirical force field and water model used. In recent years, many studies have analyzed the influences of different force fields on the simulation results obtained for nonamyloidogenic peptides. Takao et al. [49] indicated that β-hairpin conformations are favored the GROMOS96 43A1 force field. Manuel et al. [50] suggested that there was an apparent consensus among the protein dynamics obtained when using selected variants of the AMBER, CHARMM, OPLS-AA, and GROMOS96 force fields. Dirk et al. [20] indicated that AMBER03 has a slight preference for helical conformations, whereas the GROMOS96 43A1 force field was relatively unbiased for most model peptides. However, the effects of the choice of force

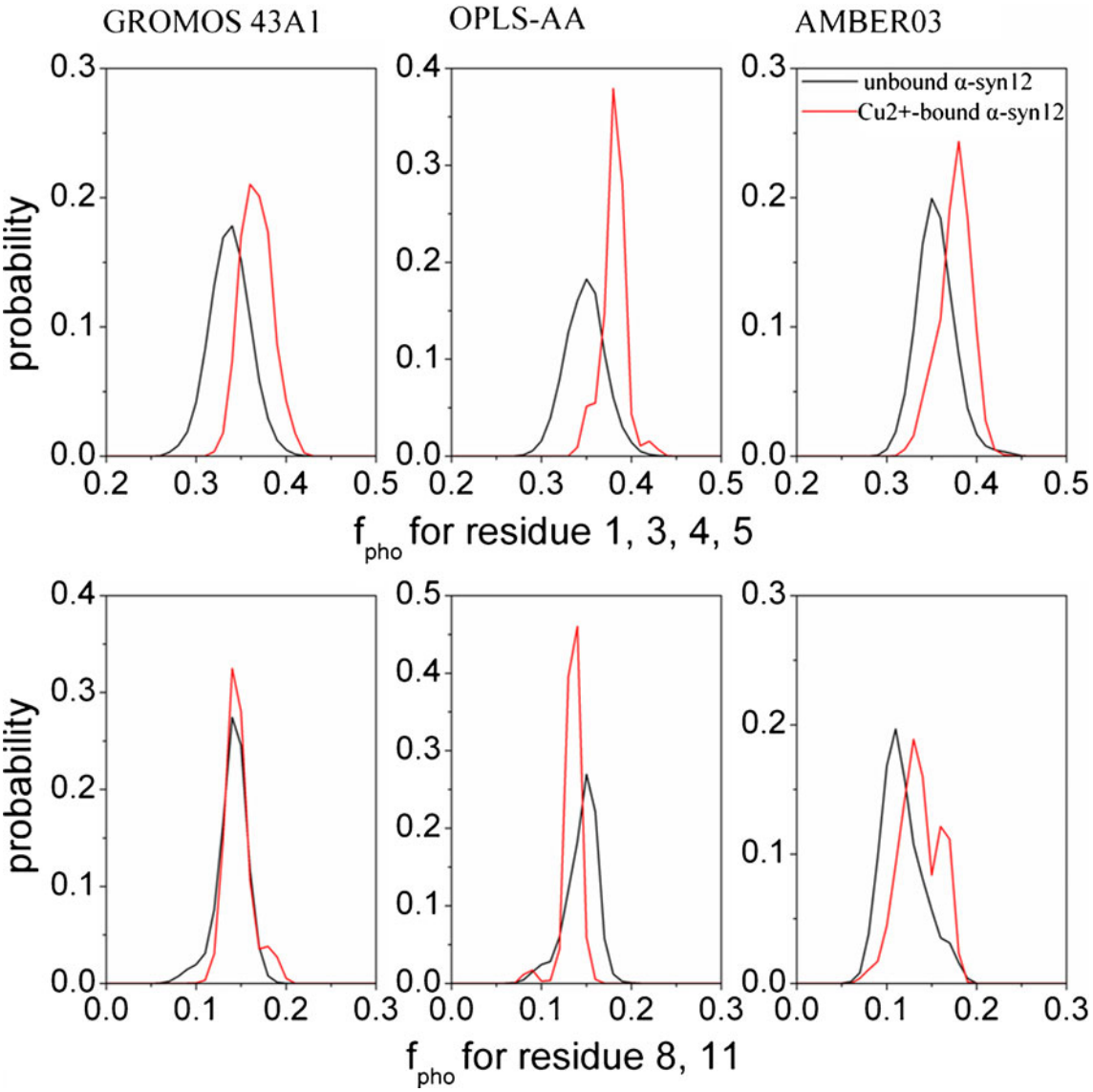

Fig. 9 Distribution of f_{pho} for: residues 1, 3, 4, and 5 (*first row*); residues 8 and 11 (*second row*)

field on the modeling results obtained for amyloidogenic peptides have been explored in only a few studies. Our early studies [29, 30] of the H1 peptide indicated that the GROMOS 43A1 force field prefers β-hairpin conformations, whereas the OPLS-AA force field prefers β-turn conformations. A study [31] of the $A\beta_{12\text{-}28}$ peptide indicated that the most densely populated conformational state is the random coil when either the GROMOS 43A1 or the OPLS-AA force field is used, which is consistent with the results of other experiments. However, the different force fields give different β-hairpins with different turns. Nguyen et al. [28] indicated that the AMBER99 force field is not suitable for exploring amyloid formation because of its strong bias towards α-helical structures, whereas the GROMOS 43A1 force field strongly favors extended β-sheet structure, and OPLS-AA yields conformations that are somewhat intermediate between those afforded by AMBER99 and GROMOS 43A1. The present study found that the AMBER03 force field has a strong bias towards α-helical structures compared with the GROMOS 43A1 and OPLS-AA force fields, whereas the GROMOS 43A1 and OPLS-AA force fields show a similar tendency to form a β-hairpin with $Turn_{9\text{-}6}$. However, the properties of local minima conformations obtained by GROMOS 43A1 and OPLS-AA differ markedly. Unfortunately, due to an absence of experimental data, it is difficult to say whether GROMOS 43A1 or OPLS-AA is more suitable for studying α-syn12 peptide.

Our simulations also indicated that the aggregation of α-syn12 peptide is stimulated by Cu^{2+} binding, which promotes the formation of a β-hairpin conformation and increases the solvent exposure of hydrophobic residues. Why does this happen? The binding site of Cu^{2+} contains (positively charged)

Asp2, which experiences electrostatic repulsion from Lys6. This makes it difficult to form $Turn_{5\text{-}2}$ and to achieve high solvent exposure of residues 1, 3, 4, and 5. Finally, Cu^{2+} modulates the conformational distribution of α-syn12 peptide from wide to narrow (which can also be thought of as moving from disorder to order), and enhances hydrophobic interactions between hydrophobic residues from different peptides.

Acknowledgments The authors thank Prof. H.J.C. Berendsen (University of Groningen) for providing us with the GROMACS programs.

This work was supported by grants 31000324, 61271378 and 30970561 from the National Natural Science Foundation of China and grants 2009ZRA14027 and 2009ZRA14028 from the Shandong Province Natural Science Foundation.

References

1. Bisaglia M, Mammi S, Bubacco L (2009) FASEB J 23:329–340
2. Yoon J, Jang S, Lee K, Shin S (2009) J Biomol Struct Dyn 27:259–270
3. Yoshiki Y, Masami M, Hiroaki S, Takashi N, Shinya H, Shin-ichi H, Koichi K, Masato H (2010) J Mol Biol 395:445–456
4. Uversky VN, Li J, Fink AL (2001) J Biol Chem 276:44284–44296
5. Rasia RM, Bertoncini CW, Marsh D, Hoyer W, Cherny D, Zweckstetter M, Griesinger C, Jovin TM, Fernandez CO (2005) Proc Natl Acad Sci USA 102:4294–4299
6. Paik SR, Shin HJ, Lee JH, Chang CS, Kim J (1999) Biochem J 340 (Pt 3):821–828
7. Bharathi, Rao KS (2007) Biochem Biophys Res Commun 359:115–120
8. Sung YH, Rospigliosi C, Eliezer D (2006) Biochim Biophys Acta 1764:5–12
9. Drew SC, Leong SL, Pham CL, Tew DJ, Masters CL, Miles LA, Cappai R, Barnham KJ (2008) J Am Chem Soc 130:7766–7773
10. Jackson MS, Lee JC (2009) Inorg Chem 48:9303–9307
11. Binolfi A, Rodriguez EE, Valensin D, D'Amelio N, Ippoliti E, Obal G, Duran R, Magistrato A, Pritsch O, Zweckstetter M, Valensin G, Carloni P, Quintanar L, Griesinger C, Fernandez CO (2010) Inorg Chem 49:10668–10679
12. Valensin D, Camponeschi F, Luczkowski M, Baratto MC, Remelli M, Valensin G, Kozlowski H (2011) Metallomics 3:292–302
13. Lee JC, Gray HB, Winkler JR (2008) J Am Chem Soc 130:6898–6899
14. Binolfi A, Lamberto GR, Duran R, Quintanar L, Bertoncini CW, Souza JM, Cervenansky C, Zweckstetter M, Griesinger C, Fernandez CO (2008) J Am Chem Soc 130:11801–11812
15. Ahmad A, Burns CS, Fink AL, Uversky VN (2012) J Biomol Struct Dyn 29:825–842
16. Dudzik CG, Walter ED, Millhauser GL (2011) Biochemistry 50:1771–1777
17. Riihimaki ES, Martinez JM, Kloo L (2007) J Phys Chem B 111:10529–10537
18. Miller Y, Ma B, Nussinov R (2010) Proc Natl Acad Sci USA 107:9490–9495
19. Rose F, Hodak M, Bernholc J (2011) Sci Rep 1:11
20. Matthes D, de Groot BL (2009) Biophys J 97:599–608
21. Duan Y, Wu C, Chowdhury S, Lee MC, Xiong G, Zhang W, Yang R, Cieplak P, Luo R, Lee T, Caldwell J, Wang J, Kollman P (2003) J Comput Chem 24:1999–2012
22. Best RB, Buchete NV, Hummer G (2008) Biophys J 95:L07–09
23. MacKerell AD Jr, Feig M, Brooks CL 3rd (2004) J Am Chem Soc 126:698–699
24. Kaminski GA, Friesner RA, Tirado-Rives J, Jorgensen WL (2001) J Phys Chem B 105:6474–6487
25. Todorova N, Legge FS, Treutlein H, Yarovsky I (2008) J Phys Chem B 112:11137–11146
26. Piana S, Lindorff-Larsen K, Shaw DE (2011) Biophys J 100:L47–49
27. Petra K, Alfonso DS, Michal O, Robert B (2012) Biophys J 102:1897–1906
28. Nguyen PH, Li MS, Derreumaux P (2011) Phys Chem Chem Phys 13:9778–9788
29. Cao Z, Wang J (2010) J Biomol Struct Dyn 27:651–661
30. Cao Z, Liu L, Wang J (2011) J Biomol Struct Dyn 29:527–539
31. Cao Z, Liu L, Zhao L, Wang J (2011) Int J Mol Sci 12:8259–8274
32. Hess B (2008) J Chem Theory Comput 4:116–122
33. van der Spoel D, van Drunen R, Berendsen HJC (1994) GRoningen MAchine for Chemical Simulations. BIOSON Research Institute, Groningen
34. van Gunsteren WF, Billeter SR, Eising AA, Hunenberger PH, Krüger P, Mark AE, Scott WRP, Tironi IG (1996) Biomolecular simulation: the GROMOS96 manual and user guide. Vdf Hochschulverlag AG an der ETH Zürich, Zürich
35. Berendsen HJC, Postma JPM, van Gunsteren WF, Hermans J (1981) Interaction models for water in relation to protein hydration. In: Pullman B (ed) Intermolecular forces. Reidel, Dordrecht, pp 331–342
36. Jorgensen WL, Chandrasekhar J, Madura JD, Impy RW, Klein ML (1983) J Chem Phys 79:926–935
37. Darden T, York D, Pedersen L (1993) J Chem Phys 98:10089–10092
38. Essmann U, Perera L, Berkowitz ML, Darden T, Lee H, Pedersen LG (1995) J Chem Phys 103:8577–8593
39. Bussi G, Donadio D, Parrinello M (2007) J Chem Phys 126:014101
40. Berendsen HJC, Postma JPM, van Gunsteren WF, DiNola A, Haak JR (1984) J Chem Phys 81:3684–3690
41. Sugita Y, Okamoto Y (1999) Chem Phys Lett 314:141–151
42. Patriksson A, van der Spoel D (2008) Phys Chem Chem Phys 10:2073–2077
43. Cao Z, Liu L, Wu P, Wang J (2011) Acta Biochim Biophys Sinica 43:172–180
44. Hu H, Elstner M, Hermans J (2003) Proteins 50:451–463
45. Best RB, Mittal J (2010) J Phys Chem B 114:8790–8798
46. Heinig M, Frishman D (2004) Nucleic Acids Res 32:W500–502
47. Garcia AE (1992) Phys Rev Lett 68:2696–2699
48. Dobson CM (2003) Nature 426:884–890
49. Takao Y, Yuji S, Yuko O (2004) Chem Phys Lett 386:460–467
50. Rueda M, Ferrer-Costa C, Meyer T, Perez A, Camps J, Hospital A, Gelpi JL, Orozco M (2007) Proc Natl Acad Sci USA 104:796–801